GEOPHYSICS, VOL. 72, NO. 5 (SEPTEMBER-OCTOBER 2007); P. SM107–SM114, 7 FIGS., 5 TABLES.
10.1190/1.2755945

Extension of forward modeling phase-screen code in isotropic and anisotropic media up to critical angle

James C. White[1] and Richard W. Hobbs[1]

ABSTRACT

The computationally efficient phase-screen forward modeling technique is extended to allow investigation of nonnormal raypaths. The code is developed to accommodate all diffracted and converted phases up to critical angle, building on a geometric construction method. The new approach relies upon prescanning the model space to assess the complexity of each screen. The propagating wavefields are then divided as a function of horizontal wavenumber, and each subset is transformed to the spatial domain separately, carrying with it angular information. This allows both locally accurate 3D phase corrections and Zoeppritz reflection and transmission coefficients to be applied. The phase-screen code is further developed to handle simple anisotropic media. During phase-screen modeling, propagation is undertaken in the wavenumber domain where exact expressions for anisotropic phase velocities are available. Traveltimes and amplitude effects from a range of anisotropic shales are computed and compared with previous published results.

INTRODUCTION

Early work using phase-screen dual-domain propagators modeled the transmission of acoustic waves in heterogeneous media. Before the generalization of the technique for elastic wave propagation (Wu, 1994), the approach was used to model, among other things, scattering of radio waves (Buckley, 1975), propagation of light along fiber optic cable (Feit and Fleck, 1978), and marine acoustics (Tappert, 1977). Wild and Hudson (1998) present a complementary elastic derivation to that of Wu (1994), approaching the problem from a geometric perspective; this approach yields the same set of governing equations.

The phase-screen method decimates the model space into a series of diffracting screens positioned perpendicular to the primary direction of wave propagation. Each screen represents a homogeneous slab for the purposes of transmission. Forward modeling proceeds monochromatically, and, as a result, propagation reduces to multiplication by $e^{i\sqrt{k^2-k_T^2}\Delta z}$ in the perpendicular wavenumber (k_x, k_y) domain for a slab of thickness Δz, where $k = \omega/c_0$, $k_T^2 = k_x^2 + k_y^2$, and c_0 is the average velocity of the slab. This represents propagating the wavefield across the slab, at an average slab velocity, as a function of angle.

The second part of the algorithm is a two-part spatial-domain multiplication that corrects locally for (1) phase errors caused by the reduction of a heterogeneous medium to a homogeneous one and (2) amplitude effects generated if an interface is encountered.

It is the construction of this phase-screen function $P(x,y)$ that provides the biggest challenge. It should be noted that in elastic media, at nonnormal incidence, conversions between P- and SV-waves will arise and the converted energy must be included. The governing equations for the method in elastic media, for an angular frequency ω, can be stated as

$$u^P(x,y,z_{j+1},\omega) = F^{-1}[e^{i\sqrt{k_P^2-k_T^2}\Delta z}F\{P_j^{PP}(x,y)u^P(x,y,z_j,\omega) + P_j^{SP}(x,y)u^S(x,y,z_j,\omega)\}], \quad (1)$$

and

$$u^S(x,y,z_{j+1},\omega) = F^{-1}[e^{i\sqrt{k_S^2-k_T^2}\Delta z}F\{P_j^{SS}(x,y)u^S(x,y,z_j,\omega) + P_j^{PS}(x,y)u^P(x,y,z_j,\omega)\}], \quad (2)$$

where u^P and u^S represent the P- and SV-wavefields, k_p and k_s are the P- and SV-wavenumbers, P^{mn} is the phase-screen function with m the incoming wavetype and n the outgoing wavetype, and F and F^{-1} are the forward and inverse Fourier transforms. The output of one screen becomes the input to the next.

Initially, the phase-screen approach was developed to model one-way propagation in heterogeneous media (Wu, 1994). The technique neglected backscattered energy whereas accurately modeling forward-scattering effects. However, to extend the technique to model

Manuscript received by the Editor December 6, 2006; revised manuscript received May 1, 2007; published online August 23, 2007.
[1]Durham University, Science Labs, Department of Earth Sciences, Durham, United Kingdom. E-mail: james.white@durham.ac.uk; r.w.hobbs@durham.ac.uk.

seismic acquisition, it was further developed (Xie and Wu, 1995; Xie and Wu, 1996; Wild and Hudson, 1998; Xie and Wu, 2001) to calculate reflected responses. Xie and Wu (2001) use the local Born approximation and a small-angle approximation to the one-way wave equation to construct the reflected waves. Wild and Hudson (1998) develop their approach from a geometric perspective and find that a bonus of using the ray formulation is the trivial extension to include backscattered energy. They apply approximations to the Zeoppritz reflection coefficients to the forward propagating wavefield and produce results analogous to the transmitted waves.

Xie and Wu (2001) explain that in regions where reflections are dominated by a single reflection event, neglecting reverberations caused by heterogeneities, the phase-screen technique is a perfectly applicable method for modeling two-way propagation. Xie and Wu (1996) test this approach using both 2D and 3D models (French, 1974) and find that full-waveform elastic-wave reflections derived from phase-screen methods are comparable to finite difference modeling for small to medium angles with respect to critical angle.

A full derivation of the small-angle, weak-scattering geometric phase-screen function is thoroughly explained by Wild and Hudson (1998) and is not repeated here. In this paper, we discuss the removal of the small-angle approximation and emphasize the correct phase-screen function for modeling all modes up to critical angle. The departure from modeling at small angles involves transforming the wavefield between wavenumber and spatial domains as a function of propagation angle. This requires splitting the wavefield into a series of subwavefields, which, as a whole, represent the entire useful precritical wavefield. These subsets can then be transformed separately, thus enabling 3D phase corrections to be applied spatially. This approach overcomes the usual uncertainty problem, when a global Fourier transform approach is adopted, between exclusive knowledge of the angular direction of the wavefield (i.e., where it is going) in the wavenumber domain, or the local position of the wavefield (i.e., where it is) in the spatial domain. Transferring angular information to the spatial domain allows locally exact Zoeppritz reflection and transmission coefficients to be calculated and applied.

Because propagation is undertaken in the wavenumber domain, it also offers the opportunity to develop the code to handle simple anisotropic rock types. If vertically transverse isotropic (VTI) media are assumed, velocity can be defined as a function of horizontal wavenumber. Therefore, the extension of the phase shift part of the algorithm for a VTI medium is trivial to define. Determination of the reflection and transmission coefficients for interfaces of one or more VTI media is a more complex problem. Graebner (1992) published solutions to these situations; we calculate these coefficients, so our code correctly handles isotropic and simple anisotropic propagation up to critical angle.

The phase-screen method has been used extensively to model seismic wave propagation with the advantage that it requires significantly less run time than other full-waveform techniques (e.g., finite difference, finite element). Maintaining this benefit is of primary importance during the development of more accurate phase-screen forward modeling codes. It is therefore essential to evaluate the number of transforms required on a screen-by-screen basis to produce a trade-off between run time and accuracy.

It is important to note that the backscattered energy is calculated and stored at each screen, where it can be reintroduced during propagation in the reverse direction. Several passes through the model space allow multiple arrivals to be included, because these are not implicitly modeled. This technique is fundamentally unsuitable for refraction seismology where propagation in the reverse direction is not the result of a specific reflection event. Extension of the method for postcritical refraction modeling is presented by Andriatsitohaina (2004).

WIDE ANGLE DEVELOPMENT

Phase correction

During Wild and Hudson's (1998) derivation of the spatial domain phase correction, they make two approximations. First, taking an average background velocity c_0 and a local phase velocity c the following perturbation, $c = c_0 + \delta c$, is assumed. A weak scattering approximation is applied to Snell's Law,

$$\frac{\sin \vartheta_0}{c_0} = \frac{\sin \vartheta}{c}, \tag{3}$$

which results in

$$\cos \vartheta = \cos \vartheta_0 \left(1 - \frac{\delta c}{c_0} \tan^2 \vartheta_0 \right), \tag{4}$$

where ϑ is the phase angle between the normal to the wavefront and the primary direction of propagation, and ϑ_0 is the same angle in a nonperturbed medium. This approximation is suitable in regions without large lateral velocity variations. Second, Wild and Hudson (1998) make a small-angle approximation reducing the phase correction, $\delta\phi = (t - t_0)\omega$, where t is the transit time across the perturbed slab and t_0 is the equivalent time across an unperturbed slab, from

$$\delta\phi(x,y) = - k\Delta z \frac{\delta c}{c_0}(x,y) \left(\frac{1 - \tan^2 \vartheta_0}{\cos \vartheta_0} \right) \tag{5}$$

to

$$\delta\phi(x,y) = - k\Delta z \frac{\delta c}{c_0}(x,y). \tag{6}$$

This simplification is required in previous versions of the code because the phase correction is applied as a 1D approximation, regardless of propagation direction; this enables the entire wavefield to be transformed together, removing the angular signature from the data. The correction is calculated from the difference between the local velocity and the average layer velocity.

To remove this simplification, angular information is required in equation 5. An approach has been developed that involves division of the wavefield in the wavenumber domain, then transformation of each subset of the wavefield individually, preserving information on slowness, and therefore angle of propagation (Andriatsitohaina, 2004). This angular phase correction can now be applied on a node-by-node basis, where each screen is divided into a regular distribution of nodes.

The wavefield is divided with Gaussian windows centered at regular intervals; the mean value of the window is used to calculate the slowness of that subset. Depending on the complexity of the model space, the number of wavefield subsets is varied. If the wavefield is divided into i subsets, then the jth subset, centered at k_j, will be calculated by applying equation 7 or 8 across the whole wavenumber space:

$$MULT_j = \frac{1}{\sqrt{2\pi}}\frac{1}{\sigma_{kx}}e^{-(k_j - k)^2/2\sigma_{kx}^2} \quad (7)$$

during 2D modeling, and

$$MULT_j = \frac{1}{2\pi}\frac{1}{\sqrt{\sigma_{kx}^2 + \sigma_{ky}^2}}e^{-(kx_j - kx)^2/2\sigma_{kx}^2}e^{-(ky_j - ky)^2/2\sigma_{ky}^2} \quad (8)$$

during 3D modeling, where the standard deviation σ is equal to the spacing of the Gaussian means in the subscripted direction.

Figure 1 shows how the total energy of the wavefield is preserved across the entire wavenumber space, except approaching the positive and negative Nyquist wavenumbers, where the amount of energy lost is dependent on the number of subsets created. This shows that the Gaussian windowed Fourier basis is no longer orthogonal and therefore results in some redundancy. The Gaussian window was chosen because of the benefits it offers with Fourier transform methods; it provides a robust and simple approach when altering the window spacing on a screen-by-screen basis.

Because each subset is transformed individually, greater angular accuracy can be achieved if the number of transforms is increased. In the limit, the data can be transformed on a node-by-node basis with

$$A = \sqrt{\mathrm{Re}(u(k_x,k_y,\omega))^2 + \mathrm{Im}(u(k_x,k_y,\omega))^2} \quad (9)$$

and

$$\phi = \tan^{-1}\frac{\mathrm{Im}(u(k_x,k_y,\omega))}{\mathrm{Re}(u(k_x,k_y,\omega))}, \quad (10)$$

allowing the calculation of the spatial wavefield $u(x,y,\omega)$ from the wavefield in the wavenumber domain $u(k_x,k_y,\omega)$ by

$$u(x,y,\omega) = Ae^{-i(k_x x + k_y y + \phi)}. \quad (11)$$

Exact angular information is now available, because the angle of incidence can be calculated from

$$\sin\vartheta = \frac{k_T c_0}{\omega}. \quad (12)$$

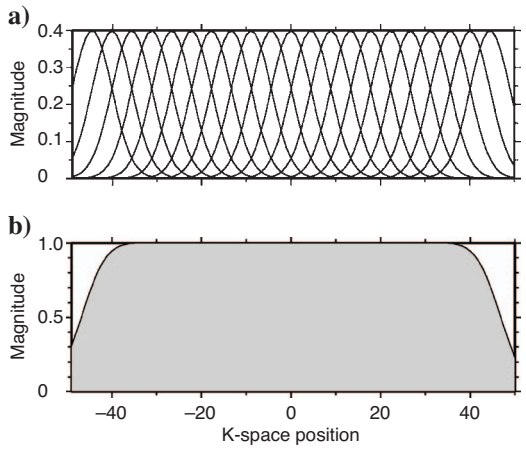

Figure 1. Distribution of 21 Gaussian subsets on a 2D, 100 node screen in the wavenumber domain. (a) The spacing and position of the distributions; (b) the summation of the Gaussian subsets, showing loss of energy only at wavenumbers close to the Nyquist limit, where the wavefield is already damped to reduce Gibbs phenomena.

Application of equation 5 on a subset-by-subset basis gives the correct phase correction for all propagating energy. It is, however, important to note that the propagation of the wavefield between screens is still applied as a single global propagation. It is the recombining of the wavefield prior to propagation that allows realistic run times to be achieved with the new approach.

Amplitude correction

The Zoeppritz (1919) equations derive the exact expressions for plane-wave reflection and transmission coefficients at a plane interface. Previous phase-screen codes have relied on normal incidence approximations to calculate the partitioning of energy at an interface (Wild and Hudson, 1998; Wild et al., 2000). However, removal of the small-angle approximation determines that it is inappropriate to use simplified equations for reflection and transmission and that the amplitude correction must be calculated as a function of angle. Adopting the approach of Sheriff and Geldart (1995), we calculate systems to define interfaces between two elastic media: an elastic medium and a fluid, and two fluid media. These solutions are exact in regions where the assumptions implicit in their derivation are valid. However, it is unlikely that plane interfaces will always be encountered, so it should be noted that the phase-screen technique is still an approximate full elastic-waveform method and the Zoeppritz solutions provide a significant improvement on previous phase-screen modeling procedures for calculating energy partitioning. By considering the geometric approach (Wild and Hudson, 1998), we remove some of the approximations inherent in the derivation to provide a more accurate technique for modeling reflection seismics.

Following a lower-upper decomposition technique for a range of incidence angles up to critical angle, a look-up table is created for every interface encountered. Application of locally exact reflection and transmission coefficients results in four outgoing wavefields (Tpp, Rpp, Tps, and Rps) for each P-wave subset, which are then summed over the entire angular model space to compute the corrected wavefields from each screen. It is important to remember that the reflection and transmission coefficients are calculated by assuming a locally plane interface between the two distinct rock types at the spatial node of the interface. Even with variation in rock properties along the screen, the exact coefficients are applied as a function of wavenumber and no approximations are required at this stage.

To provide an example of how different subsurface scenarios require a different distribution of Gaussian subsets, we present two complementary examples; both model the reflection from a planar interface between a salt layer and overlying sediment. The first example (scenario A) results in a P-P reflection coefficient that remains relatively constant prior to deviation at critical angle. The second example (scenario B) results in a steadily varying P-P reflection coefficient where a polarity inversion is encountered as angle of incidence increases. Tables 1 and 2 shows the rock parameters for both cases, whereas Figure 2a and b display the reflection coefficients as a func-

Table 1. Elastic parameters for rock types used in scenario A numerical example.

Scenario A	$V_{P\downarrow}$ (m/s)	$V_{S\downarrow}$ (m/s)	Density (kg/m^3)	δ	ε
Sediment	2600.0	1500.0	2200.0	0.0	0.0
Salt	4480.0	2590.0	2100.0	0.0	0.0

tion of angle for scenarios A and B, respectively. In all examples, a flat-topped Ricker wavelet was generated for the source wavelet. Peak frequencies ranged between 5 and 30 Hz.

The sediment-salt interface was positioned under 400 m of sediment, with receivers positioned on the surface at intervals of 10 m on an 11 screen, 2D model space with 200 nodes per screen, positioned every 10 m. Initially, the forward modeling ran with a single transform for each screen, then the number of Gaussians per screen was increased, and, finally, the nodes were transformed individually.

Figures 3 and 4 show the synthetic results for scenarios A and B for a single global transform; for 9, 99, and 199 wavefield subsets; and the response if each node is transformed individually. Scenario A produces comparable responses for all cases because the energy is partitioned almost identically, regardless of propagation angle. Scenario B shows how adopting an angle-dependent phase-screen approach offers insights into the variation of amplitude with angle. The single global-transform approach (Figures 3a and 4a) uses normal incidence reflection coefficients for all angles of incidence and, therefore, produces a negative polarity arrival at all receivers. Increasing the number of subwavefields increases the accuracy of the method. The response from the 199 Gaussian window transforms and the 200 node-by-node individual transforms are virtually identical. Computationally, the individual node transform method is faster; if the number of Gaussians required is comparable to the number of nodes, the best approach is to use the individual node method. In situations where P-wave arrivals are of primary importance, it is viable to set the number of Gaussians by prescanning for variation in P-P reflection coefficients between normal incidence and 80% of critical angle. The final Gaussian windowing is subjective and a more sophisticated approach is required when studying converted arrivals.

Table 2. Elastic parameters for rock types used in scenario B numerical example.

Scenario B	$V_{P\downarrow}$ (m/s^{-1})	$V_{S\downarrow}$ (m/s^{-1})	Density (kg/m^3)	δ	ε
Sediment	3000.0	2000.0	3300.0	0.0	0.0
Salt	4480.0	2590.0	2100.0	0.0	0.0

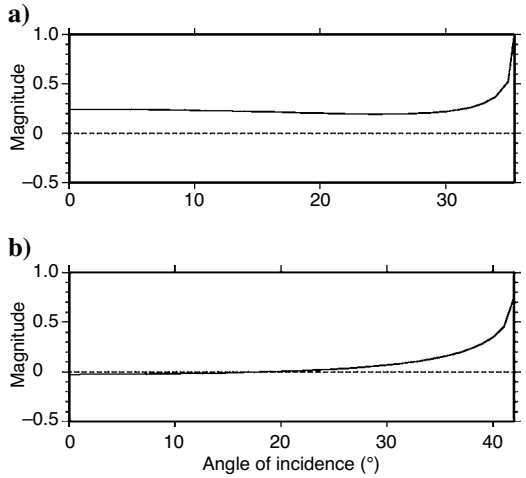

Figure 2. P-P reflection coefficients as a function of angle between normal incidence and critical angle for (a) scenario A, and (b) scenario B.

Effects of a local slope

Screens are positioned perpendicular to the primary direction of propagation, although it is unlikely that interfaces in real-earth models will be either planar or aligned with this geometry. The propagation angles computed from splitting the wavefield are relative to the screen orientation. Therefore, unless we also introduce a correction for local slope, the computational effort of producing exact arrival angles will be wasted and energy will still be partitioned incorrectly. Consequently, an approach that ascertains the local slope of an interface in 3D is developed for this study. In terms of computational run time, the optimum time to determine local slope is during the input of the model. Interfaces are tracked between adjacent nodes across a range of screens; dip and azimuth of the slope, relative to the screen geometry, are stored locally on a node-by-node basis. These are then used to determine the true arrival angle and to apply the locally correct reflection and transmission coefficients.

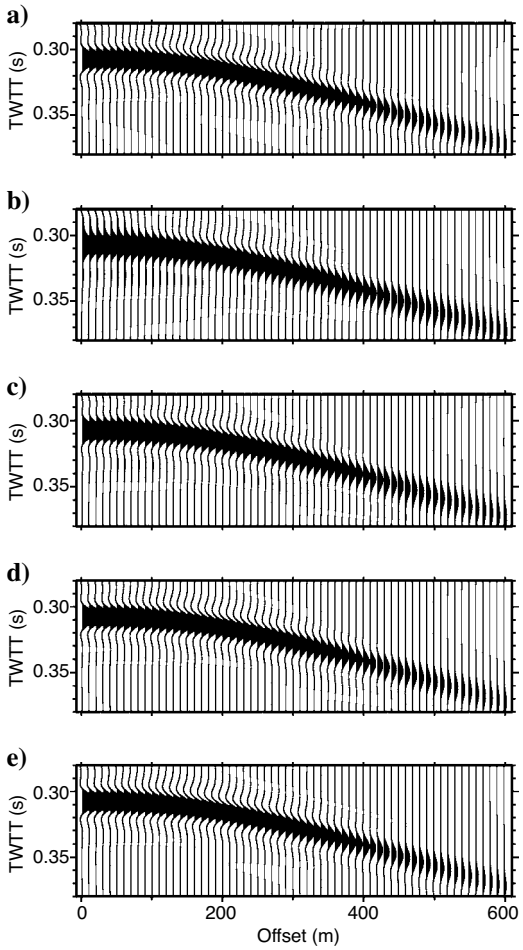

Figure 3. Synthetic seismic responses for P-P reflection from scenario A with, at each screen: (a) a single global transform of the wavefield; (b) wavefield divided into nine subsets and each transformed separately; (c) wavefield divided into 99 subsets; (d) wavefield divided into 199 subsets; and (e) wavefield transformed on a node-by-node basis. TWTT, two-way traveltime.

It should be noted that the phase-screen method is dependent on conservation of horizontal slowness from one screen to the next. Even though we now transmit and reflect the correct amount of energy, the directions of the output wavefields are not altered as a function of local slope; the slope can be thought of as a staircase. This limitation is overcome by decreasing the distance between screens and relying on the superposition of the wavefields to correct the angular direction of propagation.

Anisotropy

Wild and Hudson (1998) assumed media to be isotropic. However, it has been widely reported (e.g., Thomsen, 1986; Tsvankin and Thomsen, 1994) that during exploration, varying degrees of anisotropy are encountered. The most commonly considered anisotropic orientation is VTI, which can represent both truly anisotropic rocks and layered isotropic media, each with thicknesses less than or comparable to seismic wavelengths. The phase-screen technique lends itself to modeling propagation through VTI media as the P- and SV-wave still form a coupled system. If energy can be partitioned correctly at an interface and exact phase velocities can be calculated, then the phase-screen method can be extended to VTI systems.

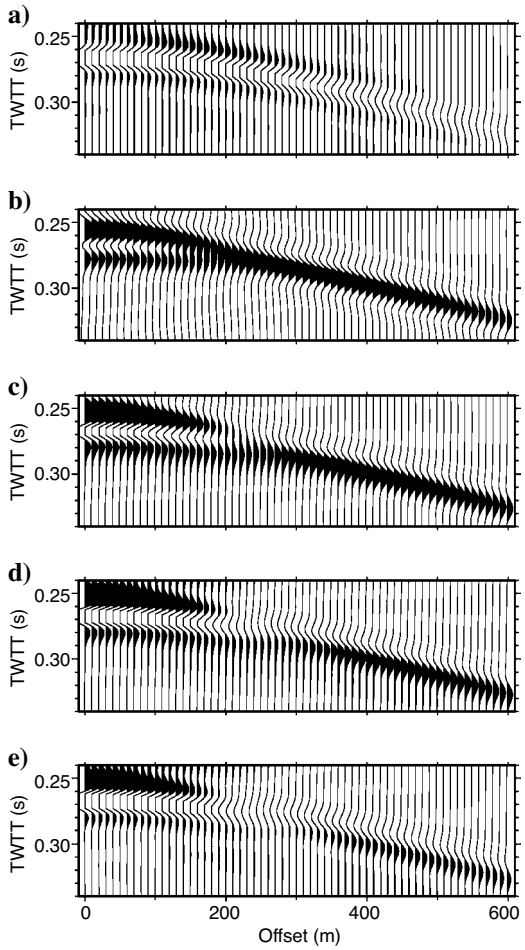

Figure 4. Synthetic seismic responses for P-P reflection from scenario B with, at each screen: (a) a single global transform of the wavefield; (b) wavefield divided into 9 subsets and each transformed separately; (c) wavefield divided into 99 subsets; (d) wavefield divided into 199 subsets; and (e) wavefield transformed on a node-by-node basis. TWTT — two-way traveltime.

Traveltimes from phase velocities

Except in symmetry planes, phase and group velocities vary in both magnitude and direction in anisotropic media. However, because propagation is undertaken in the wavenumber domain, there are exact expressions for the phase velocities. This study develops a phase-screen code for media where there is no azimuthal variation of velocity. Daley and Hron (1977) provide results for the angular variation in Q-P- and Q-SV-wave-normal velocities. Thomsen (1986) rewrote these equations in terms of his parameters (δ and ε) and these can be recast following the lead of van der Baan and Kendall (2002). Adopting their notation, we derive

$$v_P^2(k_x) = \frac{\alpha_0^2(2 - f + (\delta f - \varepsilon)\alpha_0^2 k_x^2/\omega^2 + f\sqrt{s_p})}{2 - 4\varepsilon\alpha_0^2 k_x^2/\omega^2 - 4f(\varepsilon - \delta)\alpha_0^4 k_x^4/\omega^4} \quad (13)$$

and

$$v_s^2(k_x) = \frac{\alpha_0^2(2 - f + (\delta f - \varepsilon)\alpha_0^2 k_x^2/\omega^2 - f\sqrt{s_p})}{2 - 4\varepsilon\alpha_0^2 k_x^2/\omega^2 - 4f(\varepsilon - \delta)\alpha_0^4 k_x^4/\omega^4}, \quad (14)$$

where $f = 1 - \beta_0^2/\alpha_0^2$ and

$$s_P = 1 + 4\left(\frac{2\delta - \varepsilon}{f} - \delta\right)\alpha_0^2 k_x^2/\omega^2 + 8\left(\frac{\delta^2}{2} + \delta - \varepsilon + \frac{\varepsilon - \delta - \delta\varepsilon}{f} + \frac{\varepsilon^2}{2f^2}\right)\alpha_0^2 k_x^4/\omega^4.$$

Equations 13 and 14 now provide the phase velocities as a function of wavenumber and are immediately applicable to the phase-screen technique.

Testing the propagation through VTI media using the phase-screen method

To test the traveltimes we recreate the results of van der Baan and Kendall (2002) for moveout curves associated with reflected arrivals from 1-km-thick packages of shale A and B overlying an isotropic layer (α = 4000 m/s; β = 2000 m/s; ρ = 2500 kg/m^3). We also recreate traveltimes from their multilayer model composed of an isotropic layer (α = 2000 m/s; β = 1000 m/s; ρ = 2000 kg/m^3), a package of shale B, then two more isotropic layers (α = 4000 m/s; β = 2000 m/s; ρ = 2500 kg/m^3 and α = 6000 m/s; β = 3500 m/s; ρ = 3000 kg/m^3). Each layer is 1-km thick. Table 3 shows the elastic parameters of the shales used (from Thomsen, 1986).

Figure 5 shows the moveout curves for the single-layer example with receivers positioned on the surface at intervals of 30 m on a 4 screen, 2D model space with 200 nodes per screen, and node spacing

Table 3. Elastic parameters for VTI rock types used in numerical examples.

Shale	$V_{P\downarrow}$ (m/s^{-1})	$V_{S\downarrow}$ (m/s^{-1})	Density (kg/m^3)	δ	ε
A	3368.0	1829.0	2500.0	– 0.035	0.110
B	3048.0	1490.0	2420.0	– 0.050	0.255

of 10 m. Figure 6 shows the moveout curves for the 17 screen multilayer example with the same source, receiver, and node set-up. The phase-screen method produces accurate traveltime responses whereas also delivering full waveform seismograms. In Figure 6, only the anisotropic moveout curves for the VTI layers from van der Baan and Kendall (2002) are shown.

Anisotropic reflection coefficients

The effects of anisotropy on reflection data are well known in terms of traveltime variations, but in anisotropic regions the amplitude of reflection and transmission coefficients are also affected. Thus, the application of amplitude variation with offset (AVO) analysis is important because it can provide information about rock properties. Because the subsurface is primarily anisotropic, even if only weakly, it is important to be able to quickly and successfully forward model full waveform arrivals.

The solutions for reflection and transmission coefficients between two simple anisotropic solids were initially developed by Daley and Hron (1977). Graebner (1992) published plane-wave, particle-amplitude reflection and transmission coefficients for two transversely isotropic solids in welded contact, and for a fluid overlying a transversely isotropic solid, all with vertical axes of symmetry. Starting from the wave equation in a transversely isotropic solid, the vertical phase slownesses for the Q–P– and Q–SV-waves, q_α and q_β, respectively, can be determined from the eigenvalues of the QP–QSV system:

$$q_\alpha = \frac{1}{\sqrt{2}}(K1 - \sqrt{K1 - 4K2})^{1/2} \tag{15}$$

and

$$q_\beta = \frac{1}{\sqrt{2}}(K1 + \sqrt{K1 - 4K2})^{1/2}, \tag{16}$$

where

$$K1 = \frac{\rho_1}{C} + \frac{\rho_1}{L} - \left(\frac{A}{L} + \frac{L}{C} - \frac{(F+L)^2}{CL}\right)p^2$$

and

$$K2 = \frac{A}{C}p^4 - \left(\frac{A}{CL} + \frac{1}{C}\right)p^2\rho + \frac{1}{CL}\rho^2.$$

A, F, C, and L are elastic parameters. Wright (1987) provides relationships between A, C, and L and horizontal and vertical P- and SV-velocities, whereas F is determined from parameter δ of Thomsen (1986) and ρ is the density of the medium. Pairs of eigenvectors can be determined from each of these eigenvalues and, by applying continuity of stress and displacement across an interface, systems calculating reflection and transmission coefficients from elastic parameters and horizontal wavenumber are created. In the limit of isotropy, this system reduces to the familiar Zoeppritz (1919) equations.

Graebner (1992) also provides corresponding expressions for an interface between a VTI solid and a fluid.

Testing the anisotropic reflection and transmission coefficients

Daley and Hron (1979) produced the earliest set of standard results for reflection and transmission coefficients between two VTI media. Since then, numerous researchers have provided examples of variations in the coefficients as a function of angle (White, 1982; Wright, 1987; Rüger, 1997; Yang, 2003). There is also a considerable amount of published work regarding approximations for reflection and transmission coefficients. Thomsen (1998) discusses the development of these approximations for VTI media, whereas Blangy (1994) provides an excellent overview of this topic. Figure 7 shows our reflection coefficients superimposed on those of Yang (2003). Tables 4 and 5 display the elastic parameters for the layers.

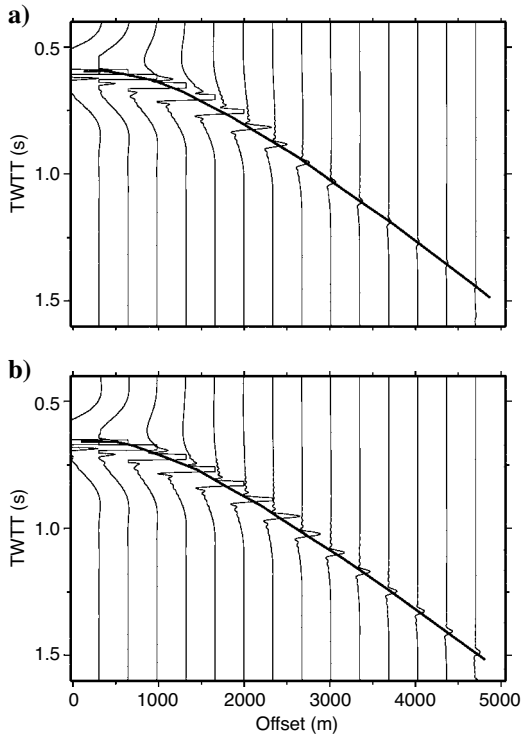

Figure 5. Moveout curves for reflected arrivals through 1 km of shale package. Traces, phase-screen modeling; line, van der Baan and Kendall (2002). (a) Propagation through shale A; (b) propagation through shale B. Elastic parameters of shales A and B are provided in Table 3. TWTT — two-way traveltime.

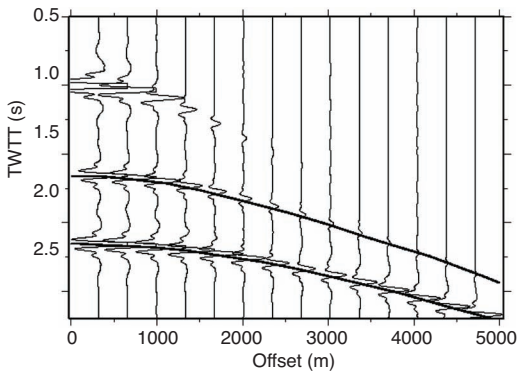

Figure 6. Moveout curves for reflected arrivals from a four-layer model. Traces, phase-screen modeling; line, van der Baan and Kendall (2002). TWTT — two-way traveltime.

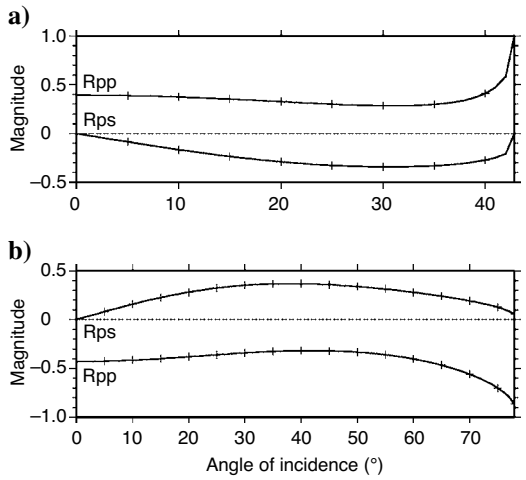

Figure 7. Examples of reflection coefficients for a VTI to isotropic interface. Bold lines, results from phase-screen code; crosses, results from Yang (2003). (a) For the case defined by Table 4, (b) for the case defined by Table 5.

Table 4. Elastic parameters for VTI reflection coefficient in Figure 7a.

	$V_{P\downarrow}$ (m/s^{-1})	$V_{S\downarrow}$ (m/s^{-1})	Density (kg/m^3)	δ	ε
Upper layer	2500.0	1250.0	1400.0	0.20	0.20
Lower layer	4000.0	2000.0	2000.0	0.00	0.00

Table 5. Elastic parameters for VTI reflection coefficient in Figure 7b.

	$V_{P\downarrow}$ (m/s^{-1})	$V_{S\downarrow}$ (m/s^{-1})	Density (kg/m^3)	δ	ε
Upper layer	6000.0	3000.0	2500.0	0.20	0.20
Lower layer	3000.0	1500.0	2000.0	0.00	0.00

CONCLUSIONS

We have presented a development of the phase-screen method, removing the narrow-angle approximation and developing a method to pass angular information between spatial and wavenumber domains. This allows nonnormal raypaths to be modeled using a phase-screen code. During this development we have adhered to the simple underlying principles of the phase-screen method, allowing us to propagate the entire useful wavefield up to critical angle. This study has also developed the technique to propagate through simple anisotropic media. This enables realistic models of the real earth to be examined, which has benefits in both forward modeling and migration.

The main challenges associated with this development are when a single screen contains both VTI and isotropic media, or if a range of VTI media are encountered in the same screen. At this time, the phase-shift propagation must be calculated at an intermediate anisotropy and the spatial phase correction must then be constructed with details of angular direction and anisotropic rock properties.

The methods described in this paper may also be applicable for other orientations of anisotropy. If the angular and azimuthal variations in velocity can be expressed as a function of horizontal wavenumber, and the P–SV-waves form a coupled system, then development of a suitable phase-screen code is possible. For horizontally transverse isotropic media, the challenge will be to calculate and store the reflection and transmission coefficients, and modeling will only be possible in the symmetry planes. During any phase-screen forward modeling, only the SV component of the full S-wavefield is considered. It should be noted that creation of a separate modeling code to handle SH-wave propagation exclusively would be possible by building on the foundations of the phase-screen method.

ACKNOWLEDGMENTS

We thank Bee Bednar, Yongzhong Wong, and two anonymous reviewers for their comments and suggestions. Research by Richard Hobbs is supported by the NERC through an Advanced Research Fellowship (NER/J/S/2002/00745). The Seismic Unix (Cohen and Stockwell, 2003) and GMT (Wessel and Smith, 1998) software packages were used to process data and create figures for this paper.

Andriatsitohaina, J. E., 2004, Accurate refraction modeling in 3-D complex isotropic media: Ph.D. thesis, University of Cambridge.
Blangy, J. P., 1994, AVO in transversely isotropic media — An overview: Geophysics, **59**, 775–781.
Buckley, R., 1975, Diffraction by a random phase-changing screen: A numerical experiment: Journal of Atmospheric and Terrestrial Physics, **37**, 1431–1446.
Cohen, J. K., and J. W. Stockwell, Jr., 2003, CWP/SU: Seismic Unix release 37: A free package for seismic research and processing: Center for Wave Phenomena, Colorado School of Mines.
Daley, P. F., and F. Hron, 1977, Reflection and transmission coefficients for transversely isotropic media: Bulletin of the Seismological Society of America, **67**, 661–675.
———, 1979, Reflection and transmission coefficients for seismic waves in ellipsoidally anisotropic media: Geophysics, **44**, 27–38.
Feit, M. D., and J. A. Fleck, Jr., 1978, Light propagation in graded-index optical fibres: Applied Optics, **17**, 3990–3998.
French, W. S., 1974, Two-dimensional and three-dimensional migration of model-experiment reflection profiles: Geophysics, **39**, 265–277.
Graebner, M., 1992, Plane-wave reflection and transmission coefficients for a transversely isotropic solid: Geophysics, **57**, 1512–1519.
Rüger, A., 1997, P-wave reflection coefficients for transversely isotropic models with vertical and horizontal axis of symmetry: Geophysics, **62**, 713–722.
Sheriff, R. E., and L. P. Geldart, 1995, Exploration Seismology, 2nd ed.: Cambridge University Press.
Tappert, F. D., 1977, The parabolic approximation method, *in* B. Keller and J. S. Papadakis, eds., Lecture notes in physics 70 — Wave propagation and underwater acoustics: Springer-Verlag.
Thomsen, L., 1986, Weak Anisotropy: Geophysics, **51**, 1954–1966.
———, 1998, Weak anisotropic reflections: *in* J. P. Castagna and M. M. Backus, eds., Offset-dependent reflectivity—Theory and practice of AVO analysis: SEG, 103–111.
Tsvankin, I., and L. Thomsen, 1994, Nonhyperbolic moveout in anisotropic media: Geophysics, **59**, 1290–1304.
van der Baan, M., and J. M. Kendall, 2002, Estimating anisotropy parameters and traveltimes in the τ-p domain: Geophysics, **67**, 1076–1086.
Wessel, P., and W. H. F. Smith, 1998, New improved version of the generic mapping tools released: EOS Transactions, **79**, 79.
White, J. E., 1982, Computed waveforms in transversely isotropic media: Geophysics, **47**, 771–783.
Wild, A. J., and J. A. Hudson, 1998, A geometrical approach to the elastic complex screen: Journal of Geophysical Research, **103**, 707–725.
Wild, A. J., R. W. Hobbs, and L. Frenje, 2000, Modelling complex media: An introduction to the phase-screen method: Physics of the Earth and Planetary Interiors, **120**, 219–255.
Wright, J., 1987, The effects of transverse isotropy on reflection amplitude versus offset: Geophysics, **52**, 564–567.
Wu, R.-S., 1994, Wide-angle elastic wave one-way propagation in heterogeneous media and an elastic wave complex-screen method: Journal of Geophysical Research, **99**, 751–766.

Xie, X.-B., and R.-S. Wu, 1995, A complex-screen method for modeling elastic wave reflections: 65th Annual International Meeting, SEG, Expanded abstracts, 1269–1272.
———, 1996, 3D elastic wave modeling using the complex screen method: 66th Annual International Meeting, SEG, Expanded abstracts, 1247–1250.
———, 2001, Modeling elastic wave forward propagation and reflection using the complex screen method: Journal of the Acoustic Society of America, **109**, 2629–2635.
Yang, J., 2003, Numerical and physical modeling of P-S converted waves in VTI media: M.Sc. thesis, University of Calgary, Canada.
Zoeppritz, K., 1919, Über Erdbebenwellen VIII B: Über Reflexion and Durchgang seismischer Wellen durch Unstetigkeitsflachen: Gottinger Nachrichten, 66–84.